INTERNATIONAL JOURNAL OF RESEARCH
In Advanced Engineering Technologies

Volume 5, Issue 3 SEP 2016

CONSTRAINED LABEL IMAGE WITH MULTIATLAS SELECTION

DR.Y.RAGHAVENDER RAO ASSOCIATE PROFESSOR AND HOD [1]

SAYAD PASHA M.TECH [2]

[1] Jawaharlal Nehru Technological University Hyderabad, College of Engineering
[2] Nachupally (Kondagattu), Jagtial, Karimnagar Dist -505501, Telangana, INDIA.

yraghavenderrao@gmail.com [1] pasha14411@gmail.com [2]

ABSTRACT

Multiatlas is commonly used in medical image segmentation. In Label Image Constrained Multiatlas Selection based image segmentation, task selection and grouping is considered as two key factors affecting the performance. Recently, various learning based atlas selection methods have emerged as very promising method. Due to the complexity of prostate structures in raw images, it is difficult to get accurate atlas selection results by only measuring the distance between raw images; it is difficult to get accurate atlas selection results by only it is difficult to get accurate atlas selection results by only measuring the distance between raw images on the manifolds. Although the distance between the regions to be segmented across images can be readily obtained by the label images, it is infeasible to directly compute the distance between the test image (gray) and the label images (binary). This paper tries to address this problem by proposing a label image constrained atlas selection method, which exploits the label images to constrain the manifold projection of raw images. Analyzing the data point distribution of the selected atlases in the manifold subspace, a novel weight computation method for atlas combination is proposed. Compared with other related existing methods, the experimental results on prostate segmentation from T2w MRI showed that the selected atlases are closer to the target structure and more accurate segmentation were obtained by using our proposed method.

Index Terms—Atlas-based, computer vision, image segmentation, manifold learning.

INTRODUCTION

PROSTATE cancer is the second cause of cancer death among American men [1]. Accurate segmentation of the prostate can be helpful for assisting the diagnosis of the prostate cancer. Traditionally, the prostate magnetic resonance (MR) image segmentations are performed manually by experts. However, manual segmentation is tedious, time consuming, and not reproducible. To overcome these shortcomings, a large number of automated image segmentation methods have been proposed [2]–[5]. Although these existing methods are effective in some cases, automated segmentation of prostate MR image is still very challenging due to the unclear boundary information in some areas [6]. As shown in Fig. 1, the red contour in the MR image on the right is a segmentation of the prostate delineated by an expert. It can be seen that the boundary is very weak in the areas indicated by the two red arrows in the original MR image in the left of Fig. 1. Experts segment these areas mainly according to their knowledge of the anatomical structure of the prostate. Therefore, it is important to use the anatomical knowledge in the automated methods.

Multiatlas based segmentation, for its full automation and high accuracy, has become one of the popular automated segmentation techniques [7]. The atlas essentially depicts the shapes and locations of anatomical structures and together

with the spatial relationships between them [8]. Thus, atlas based segmentation is one of the most common methods applied to the automated segmentation of the prostate MR image [9]–[11]. Generally, an atlas consists of a raw image and its corresponding segmented label image. In the process of multiatlas based segmentation, each atlas is first registered to the target image, resulting in a deformed atlas close to the image to be segmented. Then, a subset of atlases is selected from the deformed atlases based on certain of selection criteria. Finally, the selected atlases are combined into a single binary template for segmentation. Among the three steps of multiatlas based method, the strategy of atlas selection is one of the most critical factors affecting the accuracy of segmentation [12], [13]. Besides that, atlas combination is another important ingredient [14], where assigning the proper weight for each selected atlas is a crucial factor.

The approaches of multiatlas based segmentation can be divided into global atlas based and local atlas based. In global atlas based methods [11], [15]–[18], the measure of similarity in atlas selection and the weights assignment in atlas combination are based on the whole images. Local atlas based [19], [20] are patch-based strategies. Images are first divided into patches, and then the atlas selection and combination are both based on patches. Although the accuracy of segmentation by using local based approaches is better than using the global based approaches, local based methods brings more complicated calculation. In this paper, we mainly focus on the global atlas based method.

A. RELATED WORKS

According to the space that the procedure of atlas selection based, the existing global multiatlas based segmentation can be divided into original image space based and subspace based. In the category of original image space based methods, similarity-based selection [11], [21]–[23] is the most popular used criteria. Take the method [11] as an example, their atlas selection and combination are both based on the normalized mutual information (NMI). The atlas selection is based on measuring the similarity between images. The combination weights assignment is also according to the NMI values between test image and selected atlases. NMI evaluates the similarity between images in the original image space. Recently, manifold learning based atlas selection methods, in which the atlases can be defined as points on a manifold space to measure their similarity, have attracted a lot of attention of the researchers. A number of works [24]–[31] have shown that the medical images are embedded in a lower dimensional manifold space, and the intrinsic similarity [31] between these images can be better uncovered in this space. Based on this assumption, Wolz et al. [15] proposed an atlas selection method (LEAP) based on the lower-dimensional manifold space which is constructed by using the multidimensional scaling (MDS) [32]. However, in their atlas combination step, the computation of combination weights was also based on the original space by evaluating the NMI values between the selected atlas and test image. Similarly, our previous work [16] applied classical locality preserving projections (LPP) [33] algorithm to project the images into a manifold space for atlas selection.

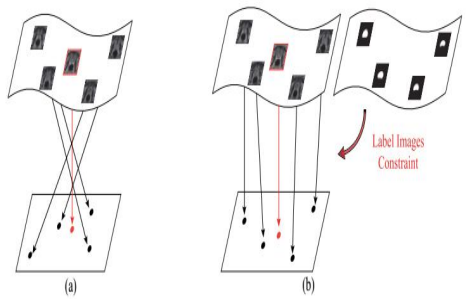

Fig. 2. (a) Misleading manifold projection due to the influence of other anatomical structures in raw images. (b) Manifold projection constrained by the label images to reduce the influence and preserve the neighborhood structure.

B. Motivation of the Proposed Method

In existing methods, others anatomical structures may affect the performance of atlas selection. For example, when segmenting the prostate from T2w MR Images delineated by the red contour as shown in Fig. 1(b), the existing manifold based methods are often distracted by the surrounding structures. Fig. 2(a) shows an example of the neighborhood structure of the prostate regions in the original high-dimensional image space. However, since the neighborhood uncovered by directly applying the manifold learning algorithms [32], [33] reflects the similarity between the entire images but not the regions to be segmented, the original neighborhood structure may not be preserved by the manifold projection using the existing methods [15], [16]. Influenced by surrounding tissues and anatomical structures, e.g., rectum and bladder, the atlas selection results might be misleading. Therefore, it is highly desirable to be able to measure the similarity between the regions of interest across images. Compared with the raw images, the shape and size information of the regions to be segmented are readily available in label images. However, directly computing the similarity between the test image (gray level) and the label images (binary) is infeasible.

In this paper, we propose a data-driven atlas selection method: label image constrained atlas selection (LICAS). The idea is to employ label images to constrain the computation of the affinity matrix of raw images in constructing the lower-dimensional manifold space, as shown in Fig. 2(b). The region of interest information from the label images is exploited together with the raw images when learning the manifold projection. Due to the constraint, the intrinsic similarity between the target regions can be uncovered in the lower-dimensional manifold space. In this space, the selected atlases are closer to the test image in terms of the regions of interest, and then the final fused template can improve the performance of the segmentation.

Based on this manifold subspace analysis, a novel weight assignment method for atlas combination is also proposed in this paper. Inspired by the work locally linear embedding (LLE) [34], the raw images and the label images of the selected atlases can be assumed to share an identical manifold structure in the lower-dimensional space. Therefore, weight assignment for the selected label images can be considered as computing the weights for the reconstruction of the data points of raw images in the manifold subspace. Then, the computed reconstruction weights can be mapped for label images for combination. Our main contributions in this paper are twofold. 1) A new manifold projection method is developed by taking the label image information into account for selecting atlases on a lower-dimensional manifold for image segmentation, which has been overlooked by other existing methods. 2) The atlas combination weights are computed by solving a problem of reconstruction of data points in the manifold subspace. To the best of our knowledge, this is the fist work that uses the label images to reduce the influence of other anatomical structures for atlas selection, and analyzes the problem of weights computation for atlas combination in a manifold subspace [16], [35]. Compared with three other recent methods

[11], [15], [16], it has been shown that our method is efficient and superior in performance. The rest of this paper is organized as follows. Firstly, the details of our proposed atlas selection method (LICAS) and the computation of atlas combination weights are presented in Sections II and III, respectively. In Section IV, we briefly describe the framework of the proposed method. The performance of the proposed method are reported and discussed in Section V. Finally, conclusions are drawn in Section VI.

II. LABEL IMAGE CONSTRAINED ATLAS SELECTION

Ideally, the atlas selection method should measure the similarity between only the regions of interest across images. Thus, a "good" manifold projection should not only preserve the neighborhood of the original manifold of raw images, but also consider the intrinsic similarity between the regions of interest. Therefore, the label image constrained atlas selection method is proposed as follows.

Let Y = $(y_1, y_2, \dots, y_n)^T$represent data points in a d-dimensional space, where each point $y_i \in R^d$ is mapped by a projection matrix P from a raw image data point $X_{Ri} \in R^m$ in the original m-dimensional manifold (d << m) as

$$X_{Ri} \rightarrow y_i = P^T X_{Ri} \qquad (1)$$

In order to preserve the neighborhood of the original manifold of raw image in projection, the objective function of the projection is

$$P_R^* = arg\min_{P_R} \sum_{ij} (y_i - y_j)^2 S_{R_{ij}} \qquad (2)$$

Where S_R is a matrix describing the similarity between the raw images. The matrix SR acts as a penalty, if xRi and xRj are close to each other in the original manifold space, the value of SRij will be large. To minimize the energy function (2), y_i and y_j should be "close" as well. Similarly, the other matrix SL is used to construct a new projection objective function for label image as

$$P_L^* = arg\min_{P_L} \sum_{ij} (y_i - y_j)^2 S_{L_{ij}} \qquad (3)$$

Where SL describes the similarity between label images. Since the shape and size information of the regions to be segmented are readily available in label images, SL makes the projection also uncover the intrinsic shape similarity between the regions of interest across images. In addition, the similarity metrics SR and SL are defined based on the standard spectral graph theory [36]. Both the similarity metrics are symmetric, i.e., SR ij = SRji, and SLij = SLij. The detailed definition is as below

$$S_{R_{ij}} = \begin{cases} \exp\left(-\frac{d(X_{Ri}, X_{Rj})}{t}\right) \\ 0 \end{cases}, \quad otherwise$$ if the nodes X_{Ri} and X_{Rj} are connected (4)

Where d (xRi, xRj) is the distance between the images of xRi and xRj, based on a certain image distance measure (IDM). T is a normalization parameter, and it is set to 1, empirically. The other matrix SL is defined in the same way as SR, according to the graph constructed by label images. By adding the constraint in (3) to the original projection computation (2), a constrained manifold projection can be obtained by minimizing the following objective function:

$$arg\min_p \sum_{ij} (y_i - y_j)^2 S_{R_{ij}} + (1-\propto)(y_i - y_j)^2 S_{R_{ij}} \qquad (5)$$

Where the parameter α adjusts the importance of the raw image and the label image. Therefore, the projection matrix P can be obtained by resolving the objective function in (5) as

$$\frac{1}{2}\sum_{ij}[\propto (y_i - y_j)^2 S_{R_{ij}} + (1-\propto)(y_i - y_j)^2 S_{R_{ij}}]$$

$$= \frac{1}{2}\sum_{ij}(y_i - y_j)^2 S_{ij}$$

$$= P^T X_R D X_R^T P - P^T X_R S X_R^T P$$

$$= P^T X_R L X_R^T P \qquad (6)$$

Where S ij = αSRij + (1 − α)SLij, and XR = (xR1, . . . , xRn). D is a diagonal matrix that Dii = j Sij. L = D − S is the classical Laplacian matrix [36]. To normalize the data points in the lower-dimensional space, a scale constraint is imposed as

$$Y^T D Y = I \implies P^T X_R D X_R^T P = \mathrm{I} \qquad (7)$$

Therefore, solving the objective function (5) is equivalent to computing

$$P^* = \arg\min_p P^T X_R L X_R^T P$$

$$\text{Given } P^T X_R D X_R^T P = I \qquad (8)$$

Note that the matrices D and L are both symmetric and positive semi definite, so are the matrices XRDXR T and XRLXR T. Therefore, the vector the pi, ith column of the matrix P, can be obtained by solving the following eigen value decomposition problem:

$$X_R L X_R^T p_i = \lambda_i X_R L X_R^T p_i \qquad (9)$$

Ranking the eigenvalues of the solution of (9) to be λ1 < λ2, < . . . , < λd, the projection matrix P can be constructed by the corresponding eigenvectors of the solutions of (9), P = (p1. . . pd), and P is a m × d matrix.

Once the matrix P is obtained, the raw images can be mapped to the lower-dimensional manifold space according to (1). Then the test image data point xT can be projected into the same d-dimensional space

$$X_T \to t = P^T X_R \qquad (10)$$

Where t represents the data point of test image in the lower dimensional space, which is illustrated by the red point in Figs. 2 and 4. After that, the similarity between the regions of interest across images can be measured by computing the simple Euclidean distance from t to each yi

$$dis_i = \|t - y_i\|_2 \qquad (11)$$

Then, the atlas selection order is obtained by ranking the distance from the nearest to the farthest (dis1 < dis2 < · · · < dis n). Consequently, a subset of K atlases {Rk, Lk} can be selected according to the atlas selection order, namely dis1 < dis2 < · · · < disK.

I. SUBSPACE ANALYSIS FOR WEIGHTED COMBINATION

In atlas combination step, weight assignment for the selected atlases is also an important factor affecting the segmentation performance. In this paper, the weight computation is based on the lower-dimensional manifold subspace. The objective of combination is to make the result close to ground truth as much as possible. That is to say, the goal is to minimize the difference between the ground truth and the combination result. Therefore, the weight vector w1 can be computed as

$$W_1^* = \arg\min_{w_1} \left\| L_g - \sum_{k=1}^{K} w_{1k} L_k \right\|_2^2$$

$$\text{s.t.} \sum w_{1k} = 1, \quad w_{1k} \geq 0 \qquad (12)$$

Where {w1k, (k = 1, 2, . . . , K)} is the weight of each selected label images Lk. Lg is the segmentation ground truth of the test image. Each Lk denotes the label image of the selected atlases, and the combination result is w1kLk. However, due to the two variables w1 and Lg are both unknown, (12) cannot be directly

solved by simultaneously estimating w1 and Lg. On the other hand, raw images are always known. Inspired by the work of locally linear embedding (LLE) [34], the raw images and the label images of the selected atlases can be assumed to be embedded in the same lower-dimensional space, as shown in Fig. 3. Therefore, the challenge of atlas combination can be considered as the problem of the reconstruction of data points in the lower-dimensional manifold subspace. Corresponding to (12), the weights for reconstruction can be rewritten as

$$W_2^* = \arg\min_{w_2} \left\| t - \sum_{k=1}^{K} w_{2k} y_k \right\|_2^2$$

$$\text{s.t.} \sum w_{2k} = 1, \quad w_{2k} \geq 0 \qquad (13)$$

Apparently, this is a linearly constrained convex quadratic programming (QP) problem. It can be solved by several classical approaches [37]. Considering the w2 is not a large-scale

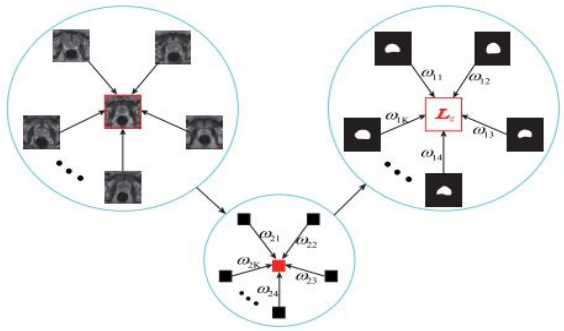

Fig. 3. Illustration of the mapping of combination weights. Assuming the raw images and the label image are embedded in the same manifold [34], the weight for combining label images combination can be computed by solving the problem of data points reconstruction in the lower-dimensional space.

vector, we applied an active-set approach [38] to solve this problem. Once the weights vector w2 is obtained, by mapping the weights vector w2 to the weights vector w1, the automatic segmentation image La can be obtained as follows:

$$L_a = \sum_{k=1}^{K} W_{1k} L_k \qquad (14)$$

Eventually, the test image T can be segmented by the obtained label image La.

II. OVERALL WORKFLOW

The workflow of the proposed method is described briefly in this section. There are three main steps in the proposed method: image preprocessing, atlases selection, and combination. The latter two steps are described in Sections II and III, respectively. For image preprocessing step, it is performed in two steps.

1) Z-Score Normalization: In order to make the different raw MR images of atlases within the same dynamic range, the classical z-score normalization [39] is employed as

$$\hat{R}_i = \frac{\check{R}_i - \mu_i}{\sigma_i} \qquad (15)$$

Where R ˇ i(i = 1, 2, . . . , N) is the raw MR image of atlases. μi is the mean of R ˇ i and σi is the standard deviation of R ˇ i. R ˆ i is the normalized image of the original image R ˇ i. For a test image T ˆ , the z-score normalization is also performed on it.

2) Registration: After image normalization, each normalized raw image of atlases R ˆ i is aligned to the normalized test image T, as shown in the left part of the first row in Fig. 4. The alignment is implemented by a 3-D rigid registration and followed by 3-D nonrigid B-spline deformable registration using the public medical image registration tool elastix [40] (using the default parameter settings). With the parameters of transformation yielded from the alignment, each atlas {R ˆ i, L ˆ i} is warped to the test image T, generating the deformed atlas {Ri, Li}.

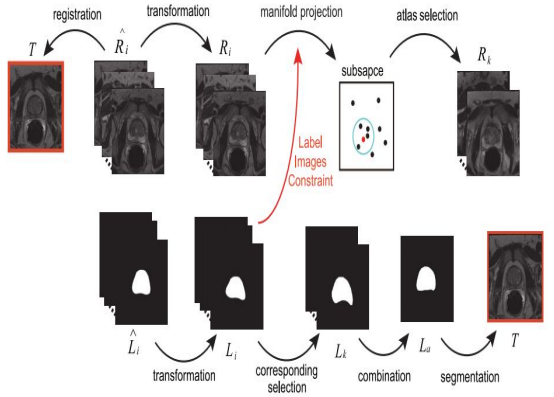

Fig. 4. Workflow of our proposed method. The upper row shows the process for analyzing the raw images of the atlases, and the lower row is the processing steps of the corresponding label images.

The complete workflow of the proposed method is illustrated in Fig. 4.

III. EXPERIMENTS

A. Materials and Evaluation Methods

The performance of the proposed method was tested on 60 T2w prostate 3-D MR images from 60 different patients obtained by using endorectal coil with 3T Philips magnetic resonance imaging (MRI) scanner. The size of each image is 512 × 512 × 26 pixels with the resolution of 0.3 mm × 0.3 mm ×3 mm. The performance of the atlas selection was measured by the overlap between the selected deformed label images of atlas and the ground truth of test image, where each ground truth was manually delineated by an experienced radiologist. Then, the performance of segmentation was evaluated subsequently by measure the overlap between the automatic segmentation results and the ground truth.

The overlap was defined by the dice similarity coefficient (DSC) value as

$$\text{DSC}\,(L_g, L) = \frac{2|L_g \cap L|}{|L_g| + |L|} \qquad (16)$$

Where L g denotes the ground truth and L represents the selected label image of atlas Lk or the automatic segmentation L a. The operator |x| is the area of region x. DSC value varies from 0 to 1. A higher value suggests more overlap and higher similarity between the target regions across the images or the more accurate segmentation performance.

B. Image Distance Measure (IDM)

To fairly compare, we employed two different kinds of IDMs for the construction of the similarity metrics SR and SL. Compared with the atlas selection of [11] and [15], we applied NMI for measuring image distance, which is denoted as LICAS-1. The distance d(xRi, xRj) of IDM for similarity metric SR1 in (4) is defined as

$$d(X_{R_i}, X_{R_j}) = 1 - NMI(R_i, R_j) \qquad (17)$$

Then the Euclidean distance is used to define the distance d(xRi, xRj) in LICAS-2

$$d(X_{R_i}, X_{R_j}) = \left\| X_i - X_j \right\|^2 \qquad (18)$$

For the similarity metric SL, LICAS-1 and LICAS-2 used the same strategy by measuring the overlap between two images to compute the distance of d(xLi, xLj), defined as

$$d(X_{L_i}, X_{L_j}) = 1 - DSC(L_i, L_j) \qquad (19)$$

Where the computation of DSC is defined as in (16).

C. Atlas Selection Results

1) Qualitative Results: Fig. 5 shows an example of the selected atlases along the atlas selection order from 1th to 10th (described in the last paragraph in Section II). Examples of the selected results based on the methods [11], [15], [16], LICAS-1 and LICAS-2 are shown in Fig. 5

from top to bottom, respectively. The red surface is the test image's ground truth Lg. The surface of each selected label image Lk,(k = 1, 2,..., 10) is shown by green surface. As seen in Fig. 5, the selected images in bottom two rows (LICAS-1s and LICAS-2s) are closer to the ground truth than the results (top three rows) based on the other three methods [11], [15], [16]. It can be seen that our proposed atlas selection method, LICAS, can improve the performance of atlas selection.

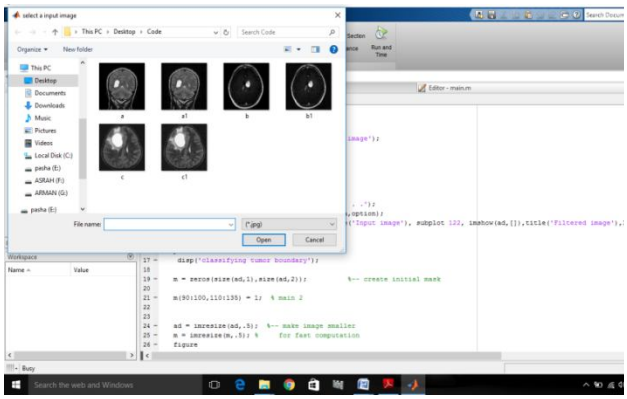

IMAGE REGISTRATION FOR SEGMENTATION

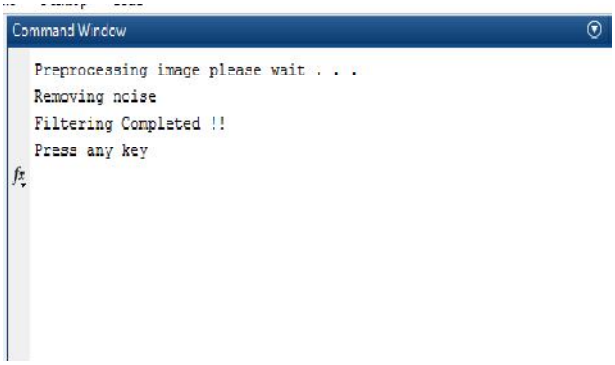

COMMAND WINDOW OF FILTERING

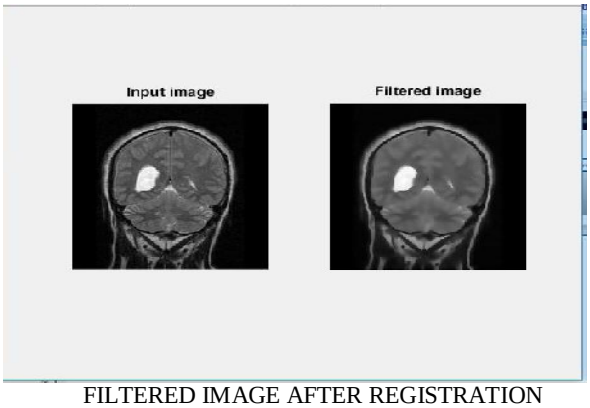

FILTERED IMAGE AFTER REGISTRATION

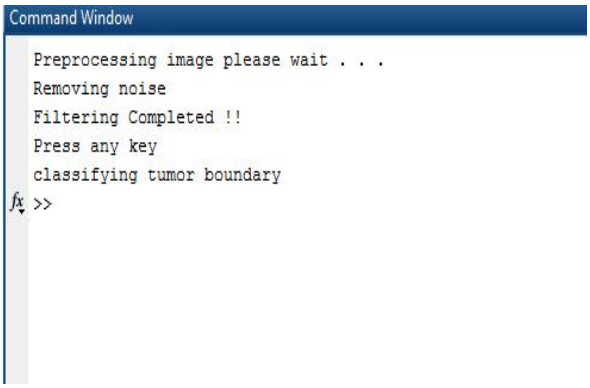

COMMAND WINDOW SELECTION FOR CLASSIFY TUMOR BOUNDARY

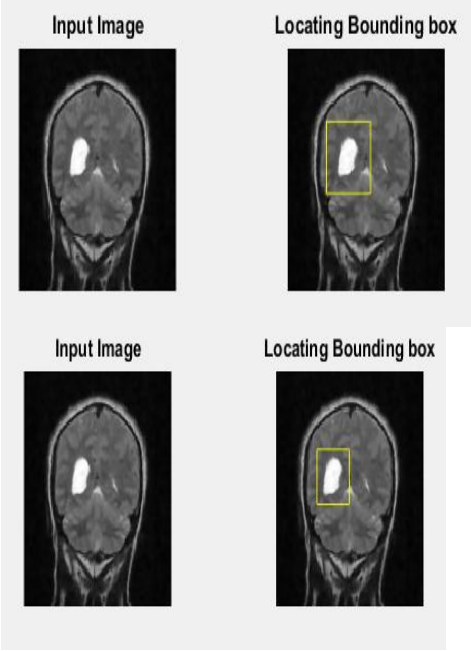

LOCATING A BOUNDARY BOX

∝		0	0.1	0.2	0.3	0.4	0.5	0.6	0.7	0.9
Average DSC	LICAS-1	0.81 20	0.81 10	0.81 11	0.80 90	0.81 04	0.81 23	0.81 09	0.81 15	0.80 84
	LICAS-2	0.81 10	0.81 05	0.81 10	0.81 15	0.81 07	0.80 98	0.80 69	0.81 00	0.80 43

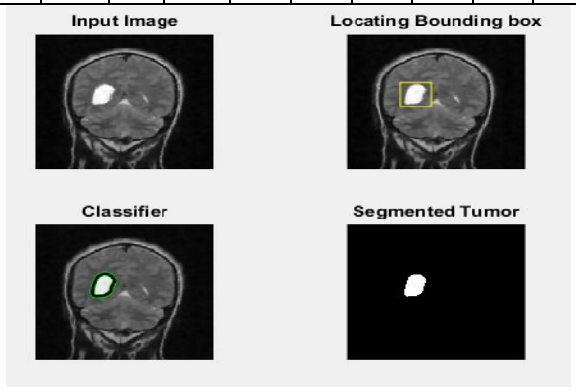

SEGMENTING THE TUMOR

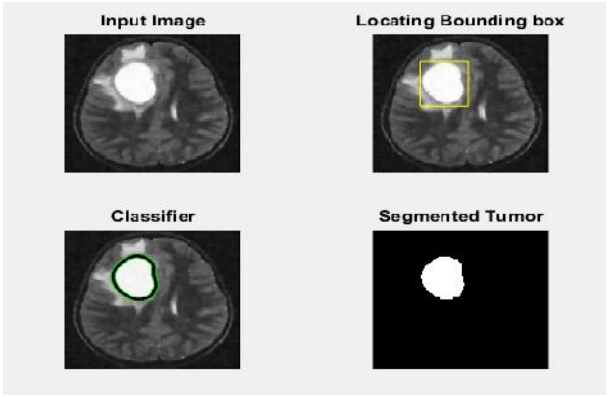

a

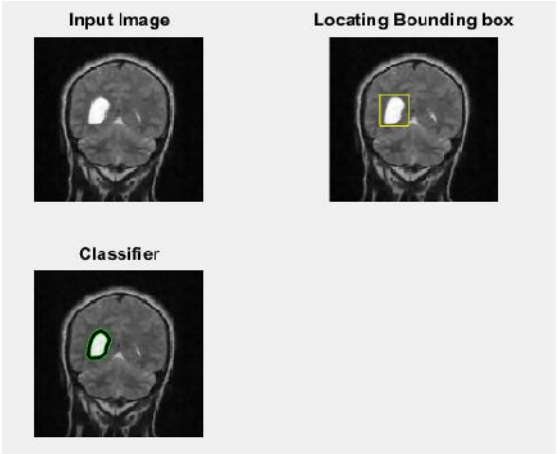

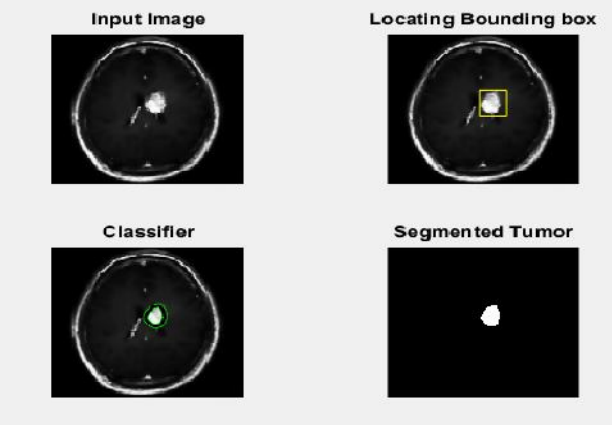

b

MULTIATALS SEGMENTATION FOR DIFFERENT IMAGES

IV. CONCLUSION

In this paper, we proposed a novel manifold learning based atlas selection method and a new weight computation algorithm for atlas combination in multiatlas based segmentation. In atlas selection step, it employs the label images to constrain the manifold projection to reduce the influence of surrounding anatomical structures in raw images. Constrained by the label images, the manifold projection is able to help uncover the intrinsic similarity between the regions of interest across images. In the step of atlas combination, the weight computation for combining the selected label images is computed by the reconstruction of data points of the selected raw images in the lower-dimensional space. By comparing with three other state-of-the-art atlas selection methods [11], [15], [16], the experimental results showed that the selected atlases are closer to the test images based on the proposed method, and the final performance of the segmentation was also improved. To the best of our knowledge, the proposed method is the first work that employs the label images to reduce the influence of other anatomical structures in raw images for atlas selection in multiatlas based segmentation, and the first method that computes the weights for atlas combination by using subspace analysis. Although the performance of atlas selection and the final segmentation has been improved compared with the existing methods [11], [15], [16], according to Fig. 10, it can been seen that the segmentation errors are much larger in the apex and caudal regions of prostate. Thus, in our future work, we will investigate the methods to improve the segmentation performance in these regions. We will also further study more efficient method to improve the performance of atlas selection and segmentation.

REFERENCES

[1] P. Yan, S. Xu, B. Turkbey, and J. Kruecker, "Discrete deformable model guided by partial active shape model for TRUS image segmentation," IEEE Trans. Biomed. Eng., vol. 57, no. 5, pp. 1158–1166, May 2010.

[2] X. Gao, B. Wang, D. Tao, and X. Li, "A relay level set method for automatic image segmentation," IEEE Trans. Syst., Man, Cybern. B, Cybern., vol. 41, no. 2, pp. 518–525, Apr. 2011.

[3] D. Pham, C. Xu, and J. Prince, "Current methods in medical image segmentation," Annu. Rev. Biomed. Eng., vol. 2, no. 1, pp. 315–337, 2000.

[4] Y. Guo, Y. Zhan, Y. Gao, J. Jiang, and D. Shen, "MR prostate segmentation via distributed discriminative dictionary (DDD) learning," in Proc. IEEE 10th Int. Symp. Biomed. Imaging (ISBI), San Francisco, CA, USA, Apr. 2013.

[5] Y. Gao, S. Liao, and D. Shen, "Prostate segmentation by sparse representation based classification," in Medical Image Computing

and Computer-Assisted Intervention–MICCAI. Berlin, Germany: Springer, 2012, pp. 451–458.

[6] N. Werghi, Y. Xiao, and J. P. Siebert, "A functional-based segmentation of human body scans in arbitrary postures," IEEE Trans. Syst., Man, Cybern. B, Cybern., vol. 36, no. 1, pp. 153–165, Feb. 2006.

[7] A. Elnakib, G. Gimel'farb, J. S. Suri, and A. El-Baz, "Medical image segmentation: A brief survey," in Multi Modality State-of-theArt Medical Image Segmentation and Registration Methodologies. New York, NY, USA: Springer, 2011, pp. 1–39.

[8] T. Rohlfing, R. Brandt, R. Menzel, D. Russakoff, and C. Maurer, "Quo vadis, atlas-based segmentation?" in Handbook of Biomedical Image Analysis. New York, NY, USA: Kluwer Academic/Plenum, 2005, pp. 435–486.

[9] S. Martin, V. Daanen, and J. Troccaz, "Atlas-based prostate segmentation using an hybrid registration," Int. J. Comput. Assisted Radiol. Surg., vol. 3, no. 6, pp. 485–492, 2008.

[10] J. Dowling, J. Fripp, P. Freer, S. Ourselin, and O. Salvado, "Automatic atlas-based segmentation of the prostate: A MICCAI 2009 prostate segmentation challenge entry," in Proc. Worskshop Med. Image Comput. Comput. Assist. Interv. II, London, U.K. pp. 17–24.

[11] S. Klein et al., "Automatic segmentation of the prostate in 3D MR images by atlas matching using localized mutual information," Med. Phys., vol. 35, pp. 1407–1417, Mar. 2008.

[12] T. Rohlfing, R. Brandt, R. Menzel, and C. Maurer, "Evaluation of atlas selection strategies for atlas-based image segmentation with application to confocal microscopy images of bee brains," Neuroimage, vol. 21, no. 4, pp. 1428–1442, 2004.

[13] P. Aljabar, R. Heckemann, A. Hammers, J. Hajnal, and D. Rueckert, "Multi-atlas based segmentation of brain images: Atlas selection and its effect on accuracy," Neuroimage, vol. 46, no. 3, pp. 726–738, 2009.

[14] X. Artaechevarria, A. Muñoz-Barrutia, and C. Ortiz-de-Solorzano "Combination strategies in multi-atlas image segmentation: Application to brain MR data," IEEE Trans. Med. Imag., vol. 28, no. 8, pp. 1266–1277, Aug. 2009.

[15] R. Wolz, P. Aljabar, J. Hajnal, A. Hammers, and D. Rueckert, "LEAP: Learning embeddings for atlas propagation," Neuroimage, vol. 49, no. 2, pp. 1316–1325, 2010.

[16] Y. Cao et al., "Segmenting images by combining selected atlases on manifold," in Medical Image Computing and Computer-Assisted Intervention—MICCAI. Berlin, Germany: Springer, 2011, pp. 272–279.

[17] S. K. Warfield, K. H. Zou, and W. M. Wells, "Simultaneous truth and performance level estimation (staple): An algorithm for the validation of image segmentation," IEEE Trans. Med. Imag., vol. 23, no. 7, pp. 903–921, Jul. 2004.

[18] T. R. Langerak et al., "Label fusion in atlas-based segmentation using a selective and iterative method for performance level estimation (simple)," IEEE Trans. Med. Imag., vol. 29, no. 12, pp. 2000–2008, Dec. 2010.

[19] P. Coupé et al., "Patch-based segmentation using expert priors: Application to hippocampus and ventricle segmentation," Neuroimage, vol. 54, no. 2, pp. 940–954, 2011.

[20] F. Rousseau, P. A. Habas, and C. Studholme, "A supervised patch-based approach

for human brain labeling," IEEE Trans. Med. Imag., vol. 30, no. 10, pp. 1852–1862, Oct. 2011.

[21] C. Studholme, D. Hill, and D. Hawkes, "An overlap invariant entropy measure of 3D medical image alignment," Pattern Recognit., vol. 32, no. 1, pp. 71–86, 1999.

[22] Q. Wang et al., "Construction and validation of mean shape atlas templates for atlas-based brain image segmentation," in Information Processing in Medical Imaging. Berlin, Germany: Springer, 2005, pp. 689–700.

[23] M. Wu, C. Rosano, P. Lopez-Garcia, C. Carter, and H. Aizenstein, "Optimum template selection for atlas-based segmentation," Neuroimage, vol. 34, no. 4, pp. 1612–1618, 2007.

[24] J. Hamm, D. H. Ye, R. Verma, and C. Davatzikos, "GRAM: A framework for geodesic registration on anatomical manifolds," Med. Image Anal., vol. 14, no. 5, pp. 633–642, 2010.

[25] S. Gerber, T. Tasdizen, S. Joshi, and R. Whitaker, "On the manifold structure of the space of brain images," in Medical Image Computing and Computer-Assisted Intervention—MICCAI. Berlin, Germany: Springer, 2009, pp. 305–312.

[26] R. Wolz, P. Aljabar, J. Hajnal, and D. Rueckert, "Manifold learning for biomarker discovery in MR imaging," in Machine Learning in Medical Imaging. Berlin, Germany: Springer, 2010, pp. 116–123.

[27] A. K. H. Duc, M. Modat, K. K. Leung, T. Kadir, and S. Ourselin, "Manifold learning for atlas selection in multi-atlas based segmentation of hippocampus," Proc. SPIE, vol. 8314, Feb. 2012, Art. ID 83140Z.

[28] M. Wang, H. Li, D. Tao, K. Lu, and X. Wu, "Multimodal graph-based reranking for web image search," IEEE Trans. Image Process., vol. 21, no. 11, pp. 4649–4661, Nov. 2012.